TRIUMF Experiment E614
Technical Note
Optimization of Muon Polarization in the M13 Beamline and E614 Detector

B. Ramadanovic, D.H.Wright TRIUMF

17 May 1999

Abstract

The results of Monte Carlo studies of the minimization of muon depolarization for three different beam tunes, five magnetic field maps and various amounts of material in the beam line, are presented. The optimum muon depolarization at the stopping target was achieved for a yoke half-length of 149 cm, and a yoke face thickness of 8 cm. No difference was found between yoke-hole radii of 15 and 20 cm. Shims on the inside of the upstream yoke face were found to significantly degrade polarization at the target. Reducing the thickness of the TEC mylar windows significantly improved the muon polarization at the target.

One of the main goals of E614 is to measure the product $P_\mu \xi$ to a precision of $< 3 \times 10^{-4}$. $1 - P_\mu$, the muon depolarization, must therefore be less than the preceding limit. This technical note summarizes attempts to minimize $1 - P_\mu$ with respect to changes in the M13 beam tune, the solenoidal field map, the shape of the solenoidal magnet yoke and the amount of material traversed by the muon beam. These studies were performed using GEANT Monte Carlo simulations which tracked the muon spin and momentum through part of the beamline and the detector.

1 Beamline and Detector Elements

The M13 beamline and E614 detector were simulated from the end of the last quadrupole magnet to the stopping target. The physical length of the last quadrupole magnet (from coil-edge to coil-edge) is 108 cm. Elements included in the simulation are shown in Fig. 1 and listed in order here from upstream to downstream:

-10 cm long Time expansion chamber (TEC) filled with DME at 20 torr
-90 cm long evacuated beam pipe
-18 cm long Variable degrader filled with mixture of Helium and Argon
-1 cm Air gap
-9 cm long helium buffer volume
-Scintillator
-Detector chambers
-Stopping target .

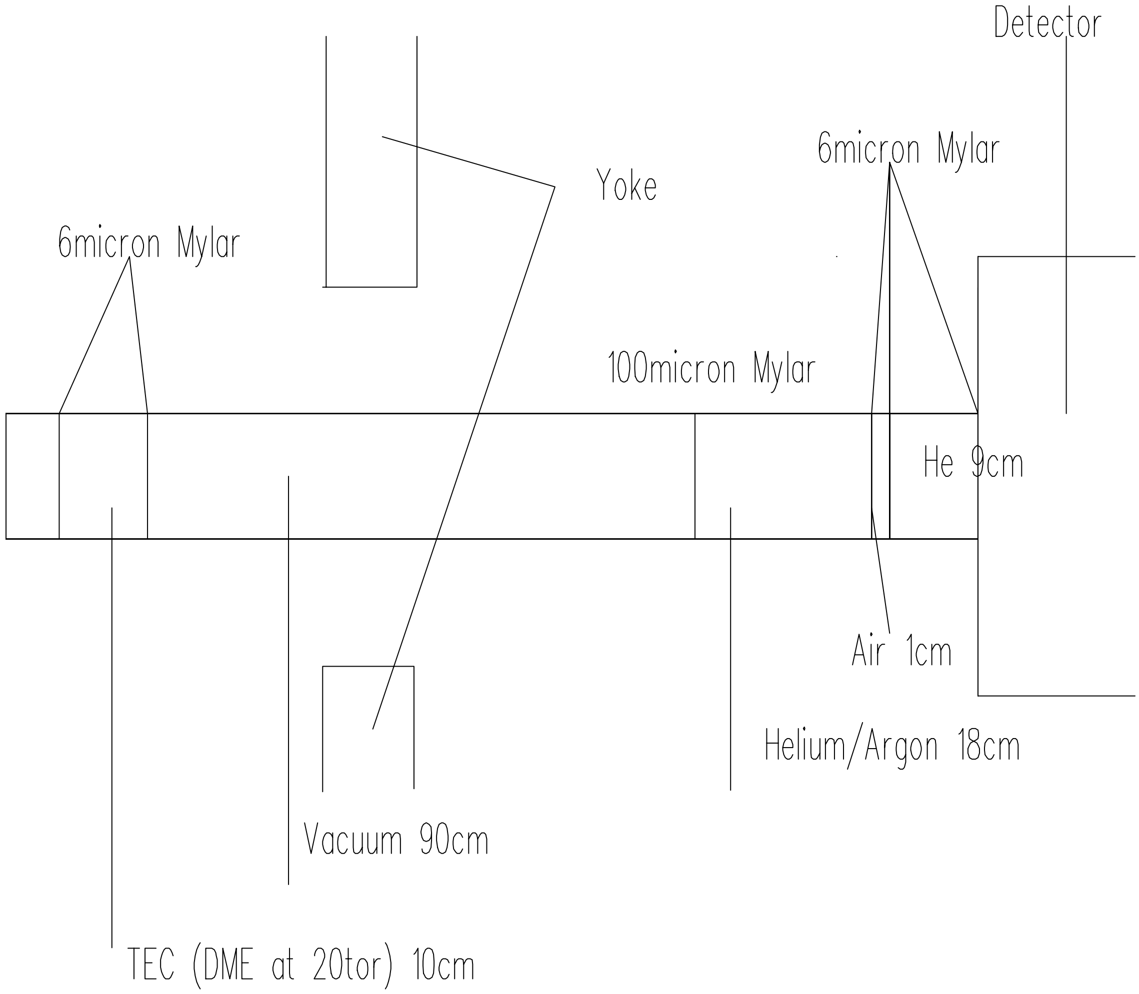

Figure 1: Geometry of M13 beamline and E614 detector used in simulation.

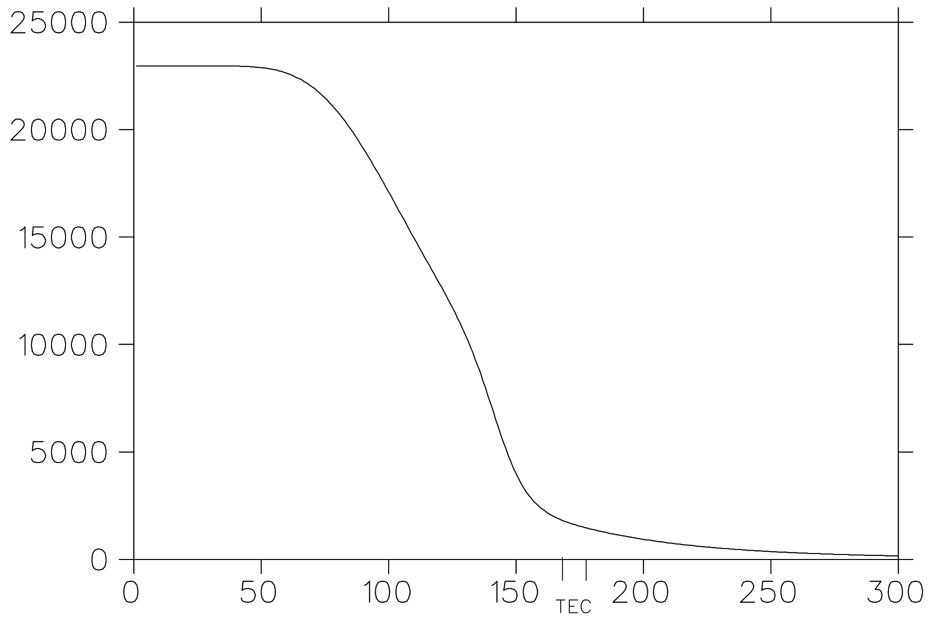

Figure 2: Longitudinal field component $B_z(z, r = 0)$ for 150 cm long yoke. The TEC is located between -180 cm and -170 cm as indicated.

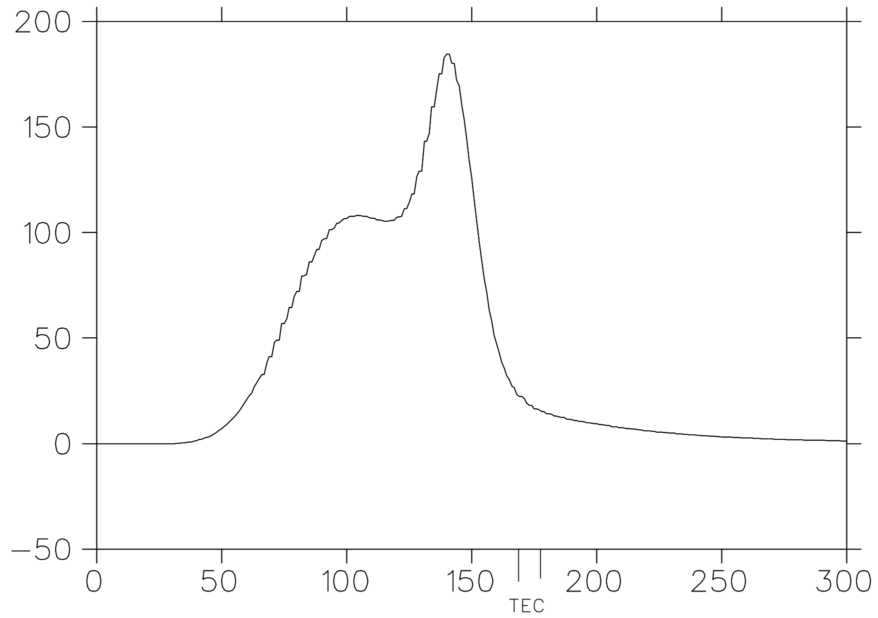

Figure 3: Radial field component $B_r(z, r = 1cm)$ for 150 cm long yoke. The TEC is located between -180 cm and -170 cm as indicated.

Time Expansion Chamber

A Time Expansion Chamber (TEC) has been proposed as a means of measuring incident muon positions and angle [1]. Large Lorentz drift angles could prevent such a chamber from working so it must be placed where the solenoidal field from the E614 magnet is relatively small. Figs. 2 and 3 show that the TEC can be placed 175 cm upstream of the stopping target without encountering large longitudinal or radial field components. The chamber is bounded upstream and downstream by 6.4 μm mylar windows except when stated otherwise below. No internal details of the TEC, other than 20 torr DME were included. For the purposes of the simulation the measured angle of the muon track was taken to be that at the center of the TEC.

Degrader (He/Ar)

An 18 cm long variable gas degrader allows control over the muon stopping distribution by varying the He/Ar mixture. In the simulations a 60%He/40%Ar mixture was used. The degrader volume was bounded on the upstream end (vacuum interface) by a 100 μm mylar foil and on the downstream end by a 6.4 μm mylar foil. The degrader was centered at 73 cm upstream of the stopping target.

Air Gap.

An air gap 1 cm long is centered at -62.5 cm. Such a gap is required in order to decouple the beamline from the main detector volume.

Buffer Helium Chamber.

A 9 cm long buffer volume was centered at -57.5 cm and was bounded by 6.4 μm mylar window upstream and downstream. Its main purpose is to protect the interior of the detector in case the 100 μm mylar window upstream should fail.

Scintillator.

A 400 μm scintillator is located in the buffer chamber. It provides particle ID information as well as additional absorber material.

Detector.

The drift and proportional chambers were of standard design as decribed elsewhere [2] .

2 Magnetic Fields and Beam Tunes Used in Simulation

Three beam tunes and five different magnetic field maps were used in the process of minimizing the muon depolarization. All of the beam tunes assumed an initial momentum of 29.7 MeV/c and a momentum spread of 0.5%. The initial muon spin was assumed to be anti-parallel to its momentum. The parameters of beam tune 1 were measured with wire chambers using a real M13 beam during an early test for E614 [3]. The parameters were: $\sigma_{\theta_x} = 6.1$ mr, $\sigma_{\theta_y} = 7.6$ mr, $\sigma_x = 4.0$ mm, $\sigma_y = 3.2$ mm. Its emittance was: $\epsilon_x = 77\pi$ mm mr and $\epsilon_y = 77\pi$ mm mr. Beam tune 2 was a REVMOC beam consisting of a file of rays [4]. It was developed as an attempt to optimize depolarization of the muons by varying M13 beamline elements. Its distributions in position and angle where roughly uniform with an x-emittance and y-emittance of 100 π mm mr. Beam tune 3 is a gaussian approximation to beam tune 2 with the same emittance. Its spatial and angular distrubutions were $\sigma_{\theta_x} = 19.1$ mr, $\sigma_{\theta_y} = 19.1$ mr, $\sigma_x = 1.73$ mm, and $\sigma_y = 1.73$ mm .

Before any of these beams were used for optimizing muon depolarization, they were tested to insure that Liouville's theorem was obeyed. The emittance proved to be conserved for all three cases, but only after transformation to canonical variables. Details on emittance calculations are given in the Appendix.

The magnetic field maps used for all tests were generated using OPERA-2D. The region mapped was $|z| \leq 300$ cm and $r \leq 30$ cm with B_z and B_r given at 1 cm intervals. Each of the following five maps represents a different yoke geometry:

A) 10 cm thick upstream yoke face placed between -170 and -160 cm in z, with a 20 cm radius hole centered on the beam axis
B) 10cm thick yoke between -150cm and -140cm with a 20 cm radius hole
C) 8cm thick yoke between -149cm and -141cm with a 15 cm radius hole
D) 8cm thick yoke between -149cm and -141cm with a 20 cm radius hole as shown at the top of Fig. 4
E) same as B) but with a 10 cm thick interior shim as shown at the bottom of Fig. 4.

Fig. 4 (top) represents the geometry labeled D but it is also a generic diagram for geometries A, B, C.

3 Results

The goal of the Monte Carlo was to find yoke designs and beam tunes which minimize the depolarization of muons at the stopping target. As a somewhat arbitrary figure of merit, a muon depolarization $(1 - S_z)$ of 2×10^{-4} was chosen. Muons with depolarizations smaller than this value were considered "useful" as they would lead to errors in $P_\mu \xi$ of less than 3×10^{-4}. This does not imply that only these muons will be used in the actual experiment. In the simulation beam muons were started 130 cm upstream of the upstream face of the magnet yoke. This was $z = -300$ cm for the long yoke design and $z = -280$ cm for the short yoke design. About 75% of these muons stop in the target at $z = 0$ with a distribution symmetric in z, as shown in Fig. 5.

The number of muons which surpass the figure of merit in each case is given below as a percentage of the number of muons stopping in the target. This percentage is strongly affected by the location of the beam focus or waist relative to the front face of the yoke. Hence the quoted percentage in each case is a result of the maximization with respect to the focus location. The optimal focus location was always found to be near the centroid of the radial field distribution. The dependence of the useful muon percentage on the focus location is shown in Table I.

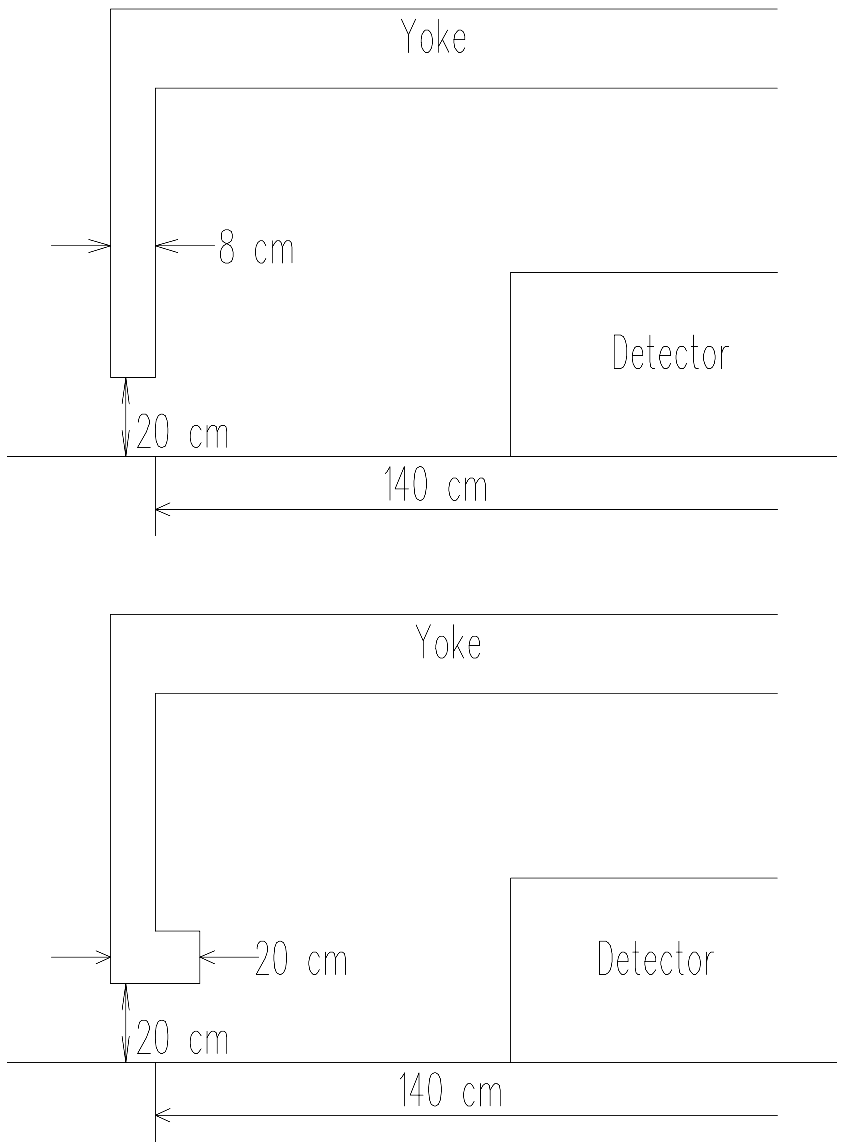

Figure 4: Typical yoke geometry without internal shims (top) and with shims (bottom).

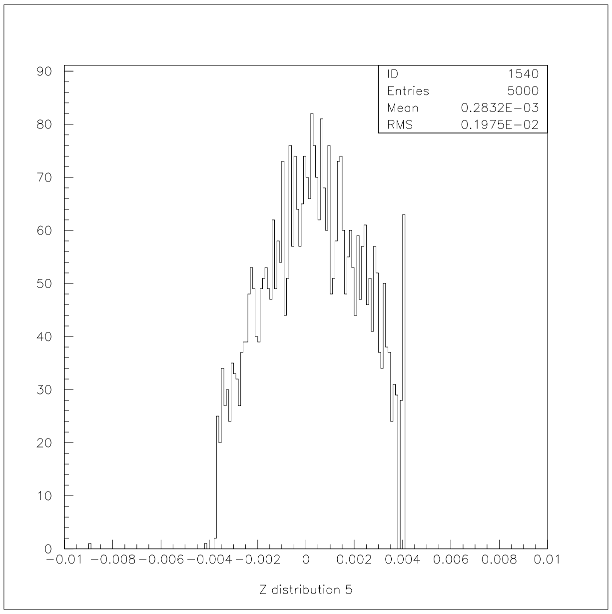

Figure 5: Stopping distribution of muons in target

Focus position z (cm)	Useful muons (%)
-120	11.5
-130	14.0
-135	14.5
-140	16.0
-143	14.0
-145	13.0
-170	5.5

Table 1: Percentage of muons stopping in target with depolarization less than 2×10^{-4} as a function of focus location. Beam tune 1 and the field from yoke design D were used. Statistical error on the percentages was $\pm$ 1.5.

Field	Beam1	Beam2	Beam3
A	16/-155	10/-150	
B	14/-130	17/-130	19/-127
C	16/-140	19/-127	22/-127
D	16/-140	20/-127	24/-127
E	05/-140	05/-127	06/-127

Table 2: Percentage of muons with depolarization below 2×10^{-4} (first entry) and optimal focus location in cm (second entry) for various beam/field combinations. Statistical uncertainty of the percentages in each case was $\pm$ 2.

The results for the beam/field combinations tested are shown in Table II. The first number in each entry represents the percentage of "useful" muons at the target and the second number is the optimal focus position.

Within statistics, results indicate that going from a yoke of half-length 170 cm (A) to one of 150 cm (B,C,D) either maintains the percentage of useful muons at the target or increases it, depending on the beam tune used. Changing the thickness of the yoke from 10 cm (B) to 8 cm (C or D) slightly improves the good muon percentage, independent of the beam tune used. The radius of the hole in the yoke does not appear to affect the good muon percentage at the target. Changing it from 20 cm (D) to 15 cm (C) alters the muon percentage by an amount less than or equal to the statistical error, depending on the beam tune. Finally the interior shims on the upstream yoke face (E) strongly degrade the good muon percentage at the target. This is due to the much stronger radial field component which comes from the extra iron near the beam axis.

A comparison of the useful muon percentage at the target was made using beam 1 and yoke design D with and without energy loss and multiple scattering in the simulation. With these processes turned off about 38% of muons stopping in the target had polarizations satisfying the figure of merit, as opposed to 20% when these processes were turned on. The reason for the difference is shown in Figs. 6 and 7. Here, the mean of the distribution of the z components of muon spin and momentum are shown as a function of the z coordinate. With energy loss and multiple scattering turned on (Fig. 6) the mass of the TEC is sufficient to increase the mean p_z component significantly. While the muon spin is not affected directly by multiple scattering, the change in momentum means that the muon will shortly be at a larger radius where the radial field will be larger. Thus the mean of the z component of the spin continues to increase along z after the muon passes the focus location. With energy loss and multiple scattering turned off (Fig. 7) the means of the z components of spin and momentum stay close to one another, as expected, and the mean of the z compenent of the spin returns to its original value as it enters the uniform field region. The above effects clearly demonstrate the need to include such processes in the optimization of any beam tune for the experiment. Routines such as REVMOC and RAYTRACE by themselves are not sufficient.

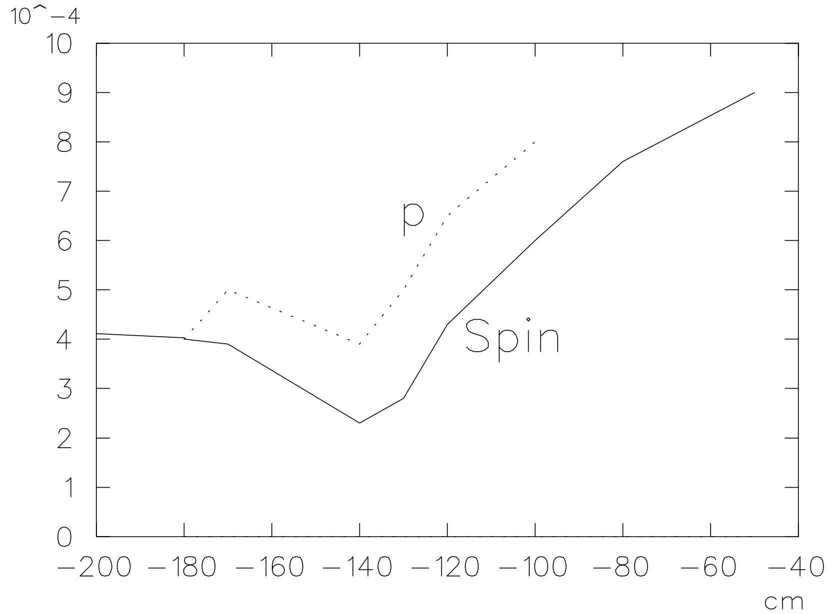

Figure 6: Mean of muon $1-S_z$ and $1-p_z/p$ as a function of z with energy loss and multiple scattering included in the simulation.

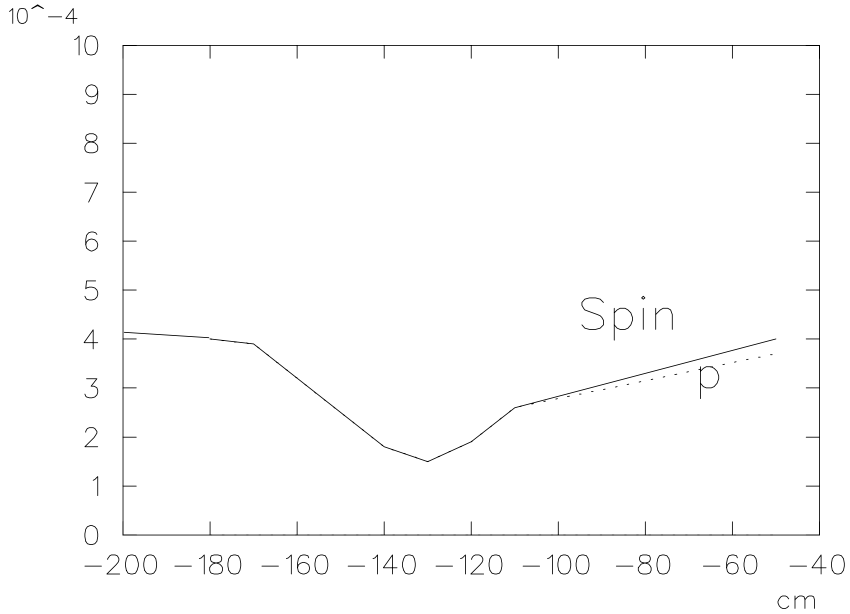

Figure 7: Mean of muon $1-S_z$ and $1-p_z/p$ as a function of z without energy loss or multiple scattering.

Wall thickness	'Useful' Muons
6.4μ	20%
2.5μ	25%
0.0μ	31%

Table 3: Percentage of useful muons at the target for 6.4, 2.5 and 0 μ thick foils. Statistical uncertanty is 1.5% for each case.

DME pressure (torr)	Useful Muons using Short TEC (10 cm)	Useful muons using Long TEC (36 cm)
0	28%	31%
20	25%	22%
50	19%	14%

Table 4: Percentage of useful muons at the target for DME lengths of 10 and 36 cm and DME pressures of 0, 20 and 50 torr. Statistical uncertanty is 1.5% for each case.

It also indicates that a reduction of the TEC mass would be very useful. Additional simulations were performed to find the effect of the mylar foil thickness on the depolarization. Because it is likely that there will be vacuum both upstream and downstream of the TEC, perhaps foils as thin as 2.5μ could be used to bound the 20 torr DME of the TEC. Table III shows the percentage of useful muons at the target for 6.4, 2.5 and 0 μ thick foils. Here, beam 2 and field map D were used. As expected a significant improvement was observed when 2.5 μ mylar foils were used. An attempt was also made to remove the downstream TEC foil and fill the adjacent vacuum pipe with 20 torr DME, but this produced no improvement in the percentage of useful muons. When the foils were removed altogether (0 μ), 10 cm of 20 torr DME remained. The resulting percentage of useful muons in that case was 31. When the DME was removed as well, this value increased to 36%, still less than the ideal case (38%) achieved with no energy loss or multiple scattering.

The effect of the DME itself was therefore seen to be significant. Simulations were performed for 10 and 36 cm lengths of DME at pressures of 0, 20 and 50 torr. The DME was bounded at each end by a 2.5 μ mylar foil. The 36 cm length was chosen because it is possible that a TEC only 10 cm long will not work well if its diameter is of the order 4 cm or more. A decision on this must await a GARFIELD study of the design. The results, shown in Table IV, can be explained in terms of two processes which produce opposite effects on the depolarization at the target. The increased amount of DME increases multiple scattering in the non-homogeneous field region, hence increasing depolarization at the target. When the longer TEC was placed in the beamline, its upstream window remained at -180 cm, while the downstream window was moved to -144 cm. With this window now deeper into the homogeneous field region the effect of multiple scattering in the window was reduced and along with it the depolarization at the target.

Almost all of the muon depolarization at the target is due to the mass of the TEC. Downstream materials contribute roughly one part in 20 to the depolarization. The largest concentration of mass downstream of the TEC is the the 100μ mylar foil between the evacuated beam pipe and the variable degrader. In an attempt to reduce the effect of the mylar the variable degrader was moved 8 cm downstream (closer to the homogeneous field region) while eliminating the buffer chamber at the entrance to the detector. Within the statistical error, this had no effect.

4 Conclusions

From the above results it was conlcuded that a yoke of half-length 149 cm and upstream face thickness of 8 cm would either maintain or improve the muon polarization at the target over the original design of 170 cm and 10 cm. Changing the radius of the beam-entry hole in the yoke from 20 cm to 15 cm did not affect the results. Shims on the interior of the faces of the yoke caused a large deterioration of the muon polarization at the target. These results were for the most part independent of the beam tune used, although there were differences from tune to tune.

The amount of material in the beam line is of course important. Reducing the thickness of the TEC mylar foils from 6.4 μ to 2.5 μ led to a significant increase in the number of useful muons at the target. Combining this change with the optimum yoke design increased the percentage of muons which stop in the target and have depolarization less than 2×10^{-4} to 25. In the ideal case of no energy loss or multiple scattering this number would be 38%. The remaining 2.5 μ foils and the 100 μ foil at the upstream end of the gas degrader account for the 13% difference. This demonstrates that any optimization of beam tunes in M13 and the E614 detector must include multiple scattering and energy loss as GEANT does.

5 Appendix - Calculating of the emittance of the beam

A stringent test of beam behavior in magnetic fields is provided by the conservation of phase space (Liouville's Theorem). To check that the beams and fields used were correct, the phase space at the initial plane was required to be equal to that at the target. Due to the presence of the magnetic field and the required transformation of canonical variables the coordinates normally used to calculate phase space in field-free space had to be changed.

The equation governing the momentum transformation is

$$\mathbf{p}' = \mathbf{p} + (q/c)\mathbf{A} \tag{1}$$

where $\mathbf{A}$ is the potential vector satisfying the equation for the magnetic field

$$\mathbf{B} = \nabla \times \mathbf{A} = (0, 0, B). \tag{2}$$

Solving for the potential we get

$$\mathbf{A} = (-1/2(By), 1/2(Bx), 0) \tag{3}$$

and therefore

$$p'_x = p_x - (qB/2c)y \tag{4}$$

$$p'_y = p_y + (qB/2c)x \tag{5}$$

$$p'_z = p_z. \tag{6}$$

Hence

$$\theta'_x = tan^{-1}(\frac{(p_x - By \cdot const)}{p_z}) \tag{7}$$

$$\theta'_y = tan^{-1}(\frac{(p_y + Bx \cdot const)}{p_z}). \tag{8}$$

Histograms of x and y as well as θ'_x and θ'_y at several z coordinates along the beamline were accumulated and the following formulae were used to obtain the emittance:

$$\epsilon_x = \sigma_x \sigma_{\theta'_x} \sqrt{1 - \frac{\sigma_{x\theta'_x}}{\sigma_x \sigma_{\theta'_x}}} \tag{9}$$

$$\epsilon_y = \sigma_y \sigma_{\theta'_y} \sqrt{1 - \frac{\sigma_{y\theta'_y}}{\sigma_y \sigma_{\theta'_y}}}. \tag{10}$$

Here σ is the root mean square of the distribution and $\sigma_{x\theta'_x}$ and $\sigma_{y\theta'_y}$ are correlations.

References

[1] Yu.I. Davydov, V.I. Selivanov and V.D. Torokhov, E614 Technical Note 17, 1998.

[2] E614 NSERC grant application, 1996 and E614 Technical Note 29, 1999.

[3] Draft of TRIUMF Review of E614, March 1994.

[4] Jaap Doornbos, private communication, 1999.